Heliyon 10 (2024) e36974

Contents lists available at ScienceDirect

Heliyon

journal homepage: www.cell.com/heliyon

Research article

The electrochemical properties of bimetallic silver-gold nanoparticles nano film's

C.O. Duya [a], F.O. Okumu [b], M.C. Matoetoe [a,*]

[a] Department of Chemistry, Cape Peninsula University of Technology, P.O. Box 1906, Bellville, South Africa
[b] Department of Physical Sciences, Jaramogi Oginga Odinga University of Science and Technology, P. O. Box 210, 40601, Bondo, Kenya

ARTICLE INFO

Keywords:
Bimetallic
Silver
Gold
Electrochemical properties

ABSTRACT

Electrode modification has been one of the most active areas of interest in electrochemistry research. Hence, the investigation of the effects of chemically and electrochemically modified GCE nano-films on the NPs electrochemical properties. The electrochemistry of nano-films of Ag NPs, Au NPs and bimetallic Ag-Au (1:2) NPs of chemical citrate reduction synthesis drop coated (DCT) and electro-deposition method (EDP) are reported. The Chemically synthesized NPs were confirmed through FT-IR, UV–visible, XRD and SEM techniques while electro-deposited NPs were ascertained by double-pulsed chrono-amperometry and electrochemical impedance spectroscopy (EIS). The nano films; GCE/Ag NPs, GCE/Au NPs and GCE/Ag-Ag (1:2) NPs in 0.1 M HCl supporting electrolyte were studied via Cyclic Voltammetry (CV) and Differential Pulse Voltammetry (DPV) techniques. Generally the DCT nano films were electrochemically superior to the EDP film in terms of current intensities and GCE/Ag-Au (1:2) NPs showed enhanced α (0.019), k_s (0.01 s^{-1}), Q (3.6×10^{-9} C), Γ (5.3×10^{-13}molescm^{-2}) and D (1.31×10^{-1} cm^{2}s^{-1}), indicating better physicochemical properties for possible sensing applications compared to electro-deposited GCE nano-films.

1. Introduction

Electrode reactions occur at the electrode/electrolyte interfaces hence, the surface chemistry and structure of the electrode play a vital role in enhancing electrode kinetics. The common electrodes are made of C, Hg, Ag and Pt [1]. Among these, carbon based electrodes such as glassy carbon (GCE) has wide applicability as a result of their broader potential window, affordability, low background current, stability and suitability in various scientific applications [2]. However, they are susceptible to fouling and non-specific redox behaviors. These challenges, are counteracted by appropriate electrode modifications using NPs. There are reports on usage of NPs nano films in sensor fabrication as well as in, electrochemical characterisation of materials, thus determining their suitability in various electrical applications [3]. Technique for modification depends on the knowledge of the fundamental electrochemistry of the electrode such as thermodynamics, mass transfer, kinetics of electron transfer, electrode surface properties and type of electrode materials [4]. The appropriate modification techniques enhances the electrochemical properties of the substrate thus tailor making it for the intended use. The electrode modification routes which have been widely reported are the chemical and electrochemical deposition [4]. The NPs adhesion processes on the electrode surface are divided into four groups; (i) electrostatic, (ii) non-specific adsorption, (iii) noncovalent and covalent [4].

* Corresponding author.
E-mail address: lellangm@gmail.com (M.C. Matoetoe).

https://doi.org/10.1016/j.heliyon.2024.e36974
Received 3 February 2024; Received in revised form 12 August 2024; Accepted 26 August 2024
Available online 28 August 2024

Chemical deposition is commonly utilised due to its ability to ensure control over the electrode surface structures [4]. This method involves introduction of NPs solution onto electrode surface mainly through drop-coating or ink mixing methods. Ink mixing methods depend on the optimized curing temperature and recipe mixture so as to ensure NPs batch reproducibility which dictates stability and sensitivity of the modified electrodes [5]-. Drop-coating method enhances electrode stability due to the placement of specified amount of NPs drops of known concentration on the electrode surface [6]. Therefore, the final concentration of NPs drop-coated can be optimized by altering the size and concentration of NPs drop-coated and dispersed in the solution. However, drop-coating is costly and susceptible to NPs aggregation hence control of NPs size and morphology becomes a challenge. Several studies involving chemical modifications of electrodes using NPs such as Bi, Pt, Rh, Au, Ag, Cu and Ni have been reported [7].

Electrochemical deposition involves reduction of metallic ions typically from NPs precursors at a fixed potential or current, electrolysis time and precursor concentration so as to obtain tailor-made NPs uniformly grown on electrode surface [8]. This process is carried out in one potentiostatic or galvanostatic step by adjusting the applied potential or current to systematically reduce the metallic ions into zero-valence state thus controlling both nucleation and growth rates [9]. This leads to the formation of NPs with improved homogeneity and sensitivity [10]. The control of NPs size and morphology can improve NPs desired attributes such as electro-catalytic properties. The method is also cost-effective because small quantities of precursors are required. It also ensures roughening of the electrode surface thus permitting better NPs adhesion on the electrode surface which in turn enhances signal generation and amplification. Electrochemical deposition has been widely applied in modifications of electrodes with bimetallic NPs using different electro-analytical techniques such as cyclic voltammetry (CV), potential step and double-pulsed chrono-amperometry (DCPA) [11]. These NPs have combinations of advantages from different metallic elements involved with minimum disadvantages of each of the metals in the resultant NPs [12]. The selection of metals electro-deposited, their order of deposition and metallic molar ratio are crucial in electrochemical synthesis of metallic NPs since they dictate the properties of the resultant NPs. Simultaneous electro-deposition of Au and Ag with improved sensitivity has been reported [13]. The structural organization of the NPs formed is determined by the differences in reduction potentials of the corresponding monometallic NPs forming the bimetallic NPs [14]. The arrangements and alignments of the monometallic atomic layers in the nanostructure formed contribute immensely to the morphology of the bimetallic NPs. Bimetallic NPs especially those synthesized from Ag, Au, Pd, Ir and Pt have been widely reported due to their improved electro-catalytic activities towards different analytes with enhanced electrode kinetics [15]. Among these, Ag and Au NPs modified electrodes have attracted attention of most researchers [16]. This is due to their rapid synthesis since both metals have closely similar lattice parameters with face-centered cubic crystal structures [17]. However, proper control of Ag-Au bimetallic NPs properties such as size, shape and morphology requires suitable control of the concentrations of Ag and Au metallic salt precursors [18]. Bimetallic Ag-Au NPs with Au: Ag ratios of 3:1 have higher electro-catalytic activity compared to those with Au: Ag ratio of 1:1 or 1:3 [19]. To the best of our knowledge, no detailed comparative study on electrochemical properties of drop-coated and electro-deposited Ag NPs, Au NPs and bimetallic Ag-Au (1:2) NPs has been reported. Therefore, in this study, Ag NPs, Au NPs and bimetallic Ag-Au (1:2) NPs were synthesized via citrate reduction and electro-deposition methods. Chemical synthesis of the NPs was confirmed through UV–visible, FT-IR, SEM and XRD techniques while electro-deposited NPs were characterized by double pulsed-chronoamperometry (DPCA). The electrochemical properties of drop-coated and electro-deposited GCE films were studied via CV and DPV techniques in 0.1 M HCl versus Ag/Ag Cl.

2. Experimental

2.1. Reagents and materials

The chemicals used were sources from *Sigma Aldrich*, South Africa. These were the precursors; Silver nitrate ($AgNO_3$, 99.9 %), gold (III) chloride trihydrate ($HAuCl_4$. $3H_2O$, 99.9 %), Reducing agent, tri-sodium citrate ($Na_3C_6H_5O_7$, 99.0 %) and the acid; hydrochloric acid (HCl, 99.9 %), nitric acid (HNO_3, 68.0 %), sulphuric acid (H_2SO_4, 98 %). Together with sodium nitrate ($NaNO_3$, 97.0 %). The 0.1 M HCl solution prepared for usage as an electrolyte in the electrochemical characterizations of the modified GCE nano-films. Deionized distilled water purified by a Milli-QTM system (18.2 MΩ cm) was used throughout the experiment for solution preparation, washing (glassware) and apparatus rinsing. Nitrogen (N_2) gas (Afrox, South Africa) was used for degassing all the electrochemical experiments. Alumina micro-powders (1.0, 0.3, 0.05 μm) and polishing pads obtained from (United Scientific, SA) were used to polish GCE. All the glass-wares and magnetic stirrers were cleaned using aqua-regia (4 HCl: 1 HNO_3) and rinsed thoroughly with the deionized distilled water before use.

2.2. Synthesis and characterization of nanoparticles

2.2.1. Chemical synthesis of nanoparticles

Ag NPs, Au NPs and bimetallic Ag-Au (1:2) NPs were synthesized using citrate reduction method. Briefly, 50 mL of $AgNO_3$ and $HAuCl_4$ were each separately heated to 240 °C under reflux and left to boil for 15 min. Followed by drop-wise addition of 1 % tri-sodium citrate (TSC) with vigorous stirring and heating for an 1 h. During which solution colour changes of yellow and purple were observed which indicated the formation of Ag and Au NPs, respectively. The synthesise of the bimetallic Ag-Au (1:2) NPs was based on co-reduction of the precursors mixture (2.5×10^{-3} M of $AgNO_3$ and 5.0×10^{-3} M of $HAuCl_4$) using 1 % TSC. The similar monomer synthesis conditions of boiling at constant temperature of 240 °C under reflux for about 15 min. Similarly a dropwise addition of 1 % TSC reducing agent followed by 1 h vigorous stirring and heating was used to ensure reduction of the precursors. The process progress was accompanied by formation of brown a coloured solution indicative of the bimetallic NPs formation. The NPs

solutions were all allowed to cool under vigorous stirring to minimize agglomeration followed by three times centrifugation purification using pure water.

2.2.2. Structural, optical and morphological characterizations of nanoparticles

The FT-IR measurements were performed using FT-IR spectrometer Spectrum Two (PerkinElmer, USA) in the spectral range of 4000-400 cm^{-1}. The sample compartment was cleaned with isopropanol followed by a background scan to minimize the effects of noise and interferences. Approximately 1 mL of each of the cleaned NPs suspensions were placed on the cleaned sample compartment and scanned sequentially.

Approximately 2 mL of pure NPs sample solutions were placed in clean quartz cuvettes for the determination of their absorbance peaks using 1800-Shimadzu UV–visible dual-beam spectrophotometer, Advanced African Technology, serial number: 127471, operated at a resolution of 1 nm in the wavelength range of 200–800 nm. The sample cuvettes were inserted in the sample compartment together with a blank cuvette containing Milli-QTM water. The baseline correction and background check were minimized using the blank thus effectively controlling interference on the NPs wavelength of interest. The spectral data was used in determining the optical band gaps of the synthesized NPs using Tauc's model [20].

The XRD data of the clean dried (room temperature (298 k) powdered NPs form was obtained using EDXRF spectrophotometer (Bruker AXS,Germany) D_8 Advanced High-Resolution diffractometer (tube voltage = 40 kV; tube current = 40 mA). The XRD spectra were recorded in the range of 10°–90° using an X-ray source of Cu-Kα (λ = 0.15406 nm) monochromatic radiation). The Spectra data was used in size calculation utilizing Debye-Scherer equation [21].

The morphology of the cleaned NPs were studied using field emission scanning electron microscopy - FE-SEMSU6600 (Hitachi, U.S.A). This was done by spreading powdered NPs samples onto adhesive tapes anchored onto metallic disks and finally covering them by thin electro-active gold films. The images of each of the NPs were acquired at same magnification and operating voltage of 5.0 kV and were analysed by image J software for sizes distribution.

2.2.3. Electrode cleaning and drop-coating of nanoparticles onto GCE

The GCE surface was cleaned sequentially using alumina micro-powders (1.0, 0.3, 0.05 μm) and polishing pads, sonicated for 10 min in ethanol/water (1:1, v/v) followed by air-drying under room temperature. The polished GCE was separately drop-coated with each of the cleaned NPs suspensions and left to dry for 2.5 h yielding stable GCE/Ag NPs, GCE/Au NPs and GCE/Ag-Au (1:2) NPs films.

2.2.4. Electro-deposition of nanoparticles onto GCE

The Cleaned GCE (as described in section 2.2.3) was dried under room temperature followed by CV running activation in 0.5 M H_2SO_4 in the potential range of −0.2 to −1.5 V for 5 cycles. Ag NPs were electro-deposited onto GCE in aqueous mixture of 5.0 mM $AgNO_3$/0.1 M $NaNO_3$ using DPCA technique. The pulse parameters applied included; $E_1 = -0.13$ V for Ag nuclei formation within 2 s followed by second pulse for growth at $E_2 = -0.26$ V, for 3 s (vs. Ag/AgCl). The electro-deposition of Au NPs was done by dipping the polished GCE in a mixture of 1.0 mM $HAuCl_4$/0.5 M H_2SO_4 followed by application of deposition potential at $E_{dep.} = -0.8$ V for 5 s. Ag-Au (1:2) NPs were electro-deposited from aqueous mixture of 1.0 mL of 1.0 mM $AgNO_3$/0.1 M $NaNO_3$ + 2.0 mL of 2.0 mM $HAuCl_4$/0.5 M H_2SO_4 by applying the first pulse at $E_1 = -0.4$ V for 2 s; and the second pulse: $E_2 = -0.7$ V for 3 s. The surfaces of each of the modified GCE nano-films were carefully cleaned with doubly-distilled water and allowed to dry at room temperature for 15 min to ensure stable nano-films for electrochemical characterizations.

2.2.5. Electrochemical characterizations of modified GCE nano-films

The impedance measurements for electrodeposited Ag, Au and Ag-Au NPs/GCE films in 0.1 M HCl versus Ag/AgCl, reference electrode were carried out using an impedance analyzer interfaced with Drop-view software for fitting and data simulation. The electrodeposited nanofilms (section 2.2.4) were allowed to dry prior to analysis. The measurements were then carried out in a frequency range of 0.1 Hz–100 kHz. To qualitatively study the electrochemical reactions at the electrolyte-electrode-NPs interface, Bode diagrams (Impedance and phase angle versus frequency) were recorded at amplitude of 50 mV. The impedance data were recorded after every minute. All the tests were performed at room temperature.

The rest of the electrochemical experiment were conducted using μStat-i 400s potentiostat: IS4091096A, serial No: 176437 (Metrohm, Spain) with NOVA software connected to a conventional three-electrode system; GCE with a diameter of 0.3 cm (A = 0.071 cm^2), Ag/AgCl (3.0 M KCl) and Pt wire from Basi as working, reference and counter electrodes, respectively. The experiments were performed at room temperature (298 K) using DPCA for investigate of nucleation and growth processes of the electro-deposited NPs while CV and DPV techniques were used for electro-activities studies of drop-coated and electro-deposited GCE nano-films in 0.1 M HCl (vs. Ag/AgCl). The data on CV and DPV was obtained at same scan rate and potential ranges (vs. Ag/AgCl) based on the electro-redox reactions of each of the GCE nano-films.

Electrochemical band gap studies were determined from the CVs Voltammograms of each of the modified nano-films in 0.1 M HCl (vs. Ag/AgCl) using Breda's equation [22]. The kinetic studies were from analysis of CV voltammograms at different scan rates ranging from 10 to 130 mVs^{-1} using *Laviron's* and *Randle's* plots obtained. These spectra were used to determine various electron transfer kinetic parameters of the NPs such as the electron transfer coefficient (α), heterogeneous rate constant (k_s), electrode surface coverage (Γ), charge contributions (Q) and diffusion coefficient (D).

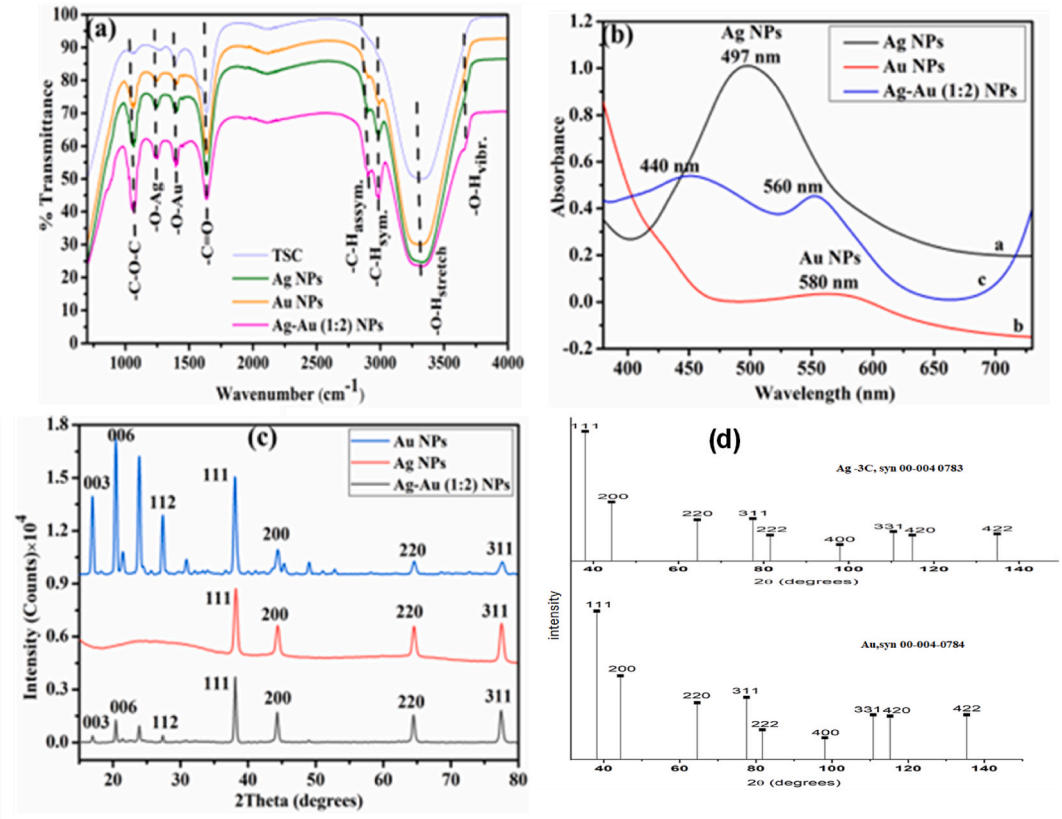

Fig. 1. An overlay spectra of chemically Synthesized Ag NPs, Au NPs and Ag-Au (1:2) NPs; (a) FT-IR, (b) UV–visible and (c) XRD and (d) JPDS spectra.

3. Results and discussion

3.1. Structural, optical and morphological characteristics of nanoparticles

The spectra overlays of FT-IR, UV–visible and XRD of chemically synthesized Ag NPs, Au NPs and bimetallic Ag-Au (1:2) NPs are depicted in Fig. 1. From Fig. 1 (a), the TSC spectrum absorption bands at 1068, 1645 and 3320 cm^{-1} from the functional group shown in the spectra are observed in all NP spectra with an increase in the absorbance/intensity at 1068, 1259 and 1420 cm^{-1} possibly as a result of an interactions between TSC and metallic ions (Ag^{+} and Au^{3+}) in the synthesized NPs. The XRD patterns of Ag NPs showed four distinct and sharp peaks of characteristic face-centered cubic (FCC) planes at 38.26° (111), 46.36° (200), 64.54° (220) and 77.55° (311) according to the JCPDS File No. 04–0783 (Fig. 1 (d)). The XRD spectrum of Au NPs showed all single peaks which were clearly distinct except the ones located at (006) and (200) crystallographic planes which possessed double peaks as a result of the close packing of the Au NPs crystals.

A small negative shift of the 2 θ accompanied suggests good Au NPs crystallinity. This shift can be attributed to enhanced d-spacing hence increased lattice volume of Au NPs. The comparison between the XRD patterns of the monometallic NPs and bimetallic Ag-Au (1:2) NPs show that the bimetallic NPs were heterogeneous mixture of Ag and highly crystalline Au NPs with distinguishable diffraction peaks at 2 θ = 38.26° (111), 46.36° (200), 64.54° (220) and 77.55° (311). This can be attributed to the presence of bulk Ag and Au with closely similar lattice parameters (Ag-0.409, Au-0.408 nm) according to JCPDS 04–0783 and 04–0784, respectively [23]. Similar results for the bimetallic NPs have also been reported [24,25].

SEM micrographs of the nanomaterials are depicted in Fig. 2. The Ag NPs micrograph comprised of semi-spherical and cuboidal-hexagonal particles with wider size distribution (10–50) nm. The particles were also poly-dispersed with smaller particles agglomerating around larger ones forming polyp-shaped clusters. This was supported by the larger particle size determined as 21.79 ± 0.79 nm. This can be attributed to agglomeration of the NPs on glass substrate during deposition process [26]. The Au NPs micrograph showed mixtures of larger cuboidal-hexagonal and relatively smaller spherical particles with rugged edges randomly distributed. The numerous smaller spherical particles coalesced into a web-like structure forming cloudy-shaped clusters. The NPs had wider size distribution (0–55 nm) with an average particle size of 19.18 ± 0.83 nm. The bimetallic NPs image Fig. 2 (c) with an EDX insert has an estimated mean diameter and narrow size distribution of 10.21 ± 0.57 nm and (0–30 nm), respectively thus indicative of particles higher dispersity with smaller-sized particles closely intertwined with relatively larger ones in chain like arrangements forming

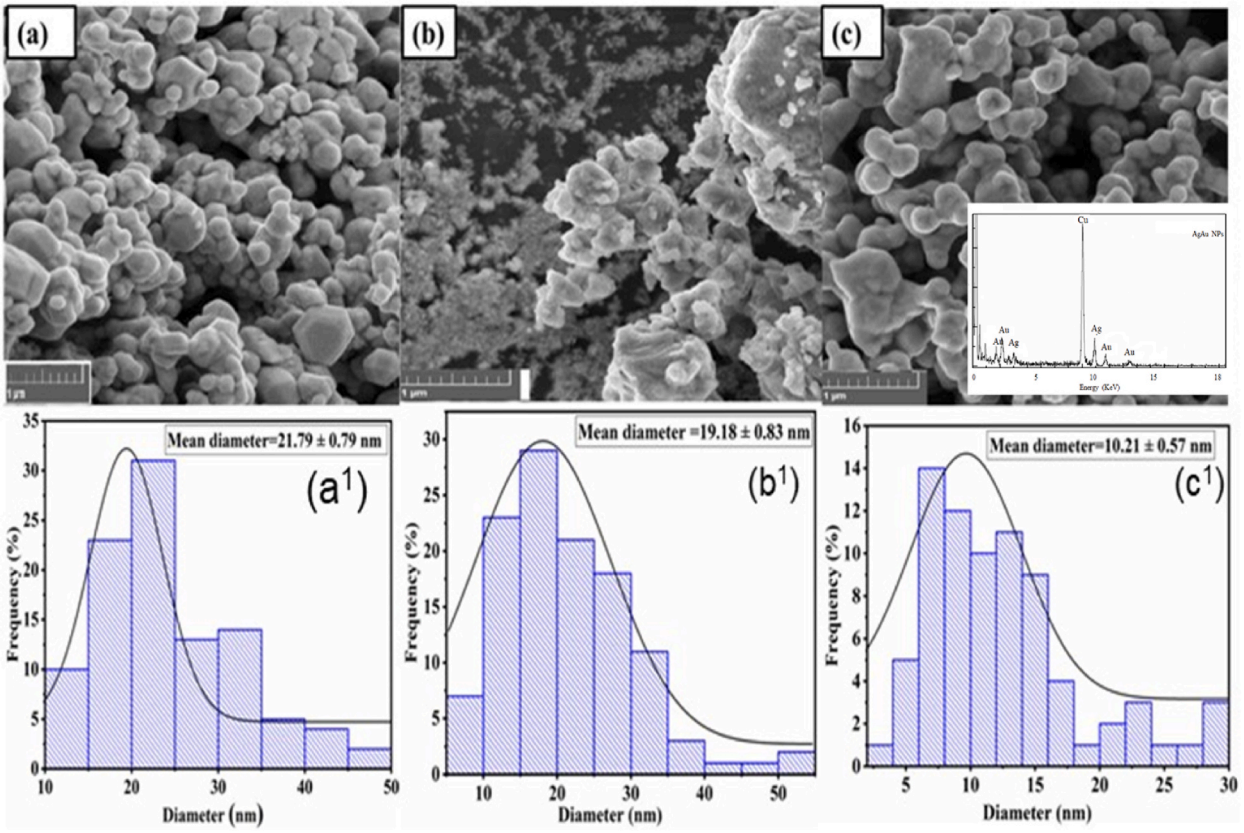

Fig. 2. Scanning electron micrographs of (a) Ag NPs, (b) Au NPs and (c) Ag-Au (1:2) bimetallic NPs with their corresponding diameter histograms; (a^1),(b^1) and (c^1) respectively.

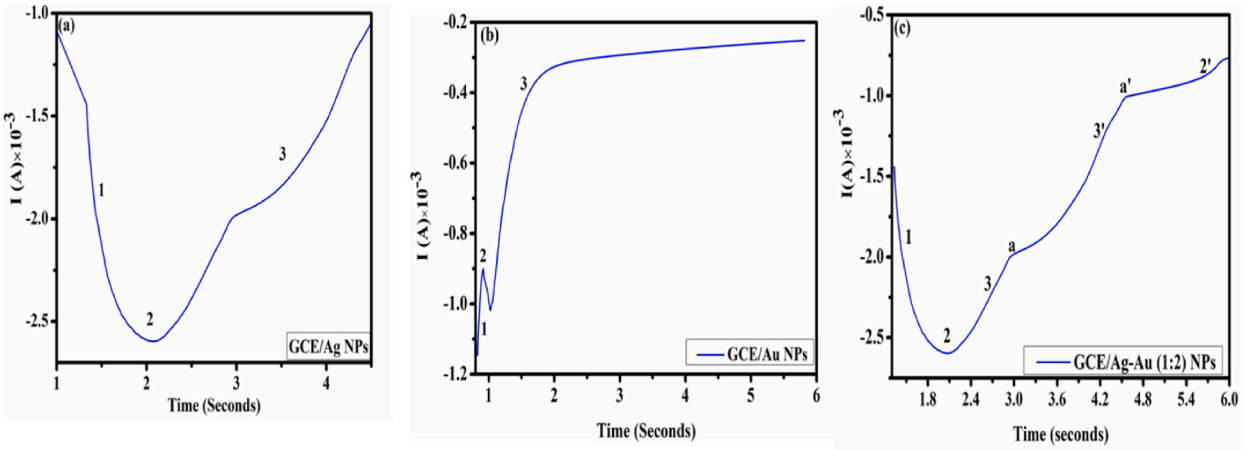

Fig. 3. Current-time (I-t) transient curves for electro-deposition of (a) Ag NPs, (b) Au NPs and (c) bimetallic Ag-Au (1:2) NPs.

cauliflower morphology. This has been similarly reported elsewhere [27]. The EDX spectrum is in agreement with the spectroscopic results in Fig. 1, showing that both Ag and Au are present.

3.2. Electro-deposition of nanoparticles onto GCE

The typical current-time (I-t) transient curves describing the systematic electro-deposition of Ag, Au and bimetallic Ag-Au (1:2) NPs, respectively onto polished GCE are as shown in Fig. 3. The curves regions labeled 1, 2 and 3 represented nucleation and growth

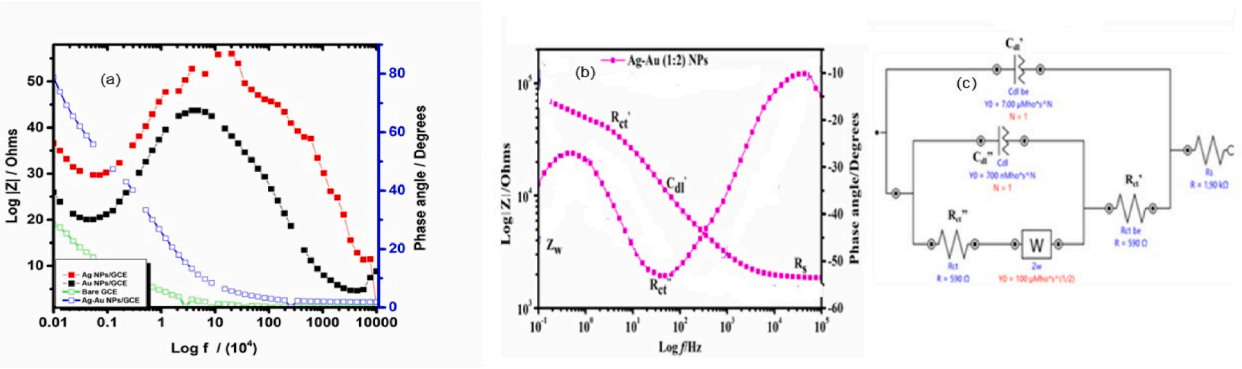

Fig. 4. The Bode plots for Ag, Au and phase angle for GCE/Ag-Au NPs films in 0.1 M HCl versus Ag/AgCl, reference electrode (a), The Nyquist presentation of the Ag-Au NPs overlayed with the phase angle (b) while the Randles equivalent circuit is depicted in (c).

processes for each of the NPs. The nucleation rates depended on concentration of metallic ions diffusing towards the electrode surface as shown in the curves.

The regions 1 and 2, show that nucleation rates increased with time between t = 1.0 and t = 2.0 s for both Ag NPs and bimetallic Ag-Au (1:2) NPs. This is accompanied by the significant increase in cathodic over-voltage with time. In contrast, the nucleation rate for Au NPs was much more rapid than that of Ag NPs leading to earlier formation of unstable Au nuclei as indicated by the slight decrease in cathodic current immediately after region 2. Thus suggesting that Au NPs nucleic growth was much slower than Ag NPs that has a sharper increase in Ag NPs peak current. Therefore, Ag nuclei were formed and deposited earlier than Au NPs. This is in agreement with the theory of nucleation [28]. Fast deposition of Ag is also supported by the small wave evident between regions 2–3 which is absent in the Au NPs curve but visible in the growth phase of the bimetallic NPs in the same region. The increase in peak current in both Ag and Au NPs curves indicated the growth of Ag and Au nuclei. The increase was sharper and longer in Au NPs compared to Ag NPs leading to the formation of mono-dispersed NPs with narrow size distribution. These indicated increased concentrations of Au^{3+}, their exposure onto the electrode surface and close inter-particle distance between the deposited Au atoms. The final flattening of the current after region 3 can possibly be ascribed to the depletion of Au precursors in the interfacial region resulting into linear diffusional conditions [29].

As evident in Fig. 3 c, immediately after region 3, the growth rate of Au increased exponentially with time. This was to prevent the system from exceeding the applied deposition potential for Au (E = −0.4 V). In region 3′, the current slightly remained constant accompanied by a small wave, **a**, which was replicated as a'. These can possibly be ascribed to the formation of Au nuclei which in turn grew over the Ag atoms as shown by the slight increase in current in region 2'. This growth process, however, did not conform to the theoretical predictions [30].

Based on the visual experimental impedance data observations of Fig. 4 there was a significant difference in impedance between the monometallic's (Ag, Au) compared to the bimetallic NPs. The data fitting average errors was less than 1 % with an acceptable *chi* square (X^2) values. The values bimetallic NPs and GCE values were; 22.32 ± 0.34 kΩ (R_{ct}), 1.91 ± 1.05 kΩ (R_s), 7.96 × 10^{-5} F (C_{DL}), 0.996 (α), 2.64 × 10^{-5} μF (Z_W). These were slightly less than the R_{CT} monometallic values of 25.40 ± 0.56 kΩ and 27.34 kΩ for Au/GCE and Ag/GCE respectively. The EIS data trend was GCE/Ag > GCE/Au > GCE/Ag-Au. A similar trend has been reported [31]. The impedance for the bimetallic NPs significantly decreased with increasing frequency, an indication of an electrochemical synergy between the monometallic's coupled with increased diffusion rates of the ions from the bimetallic NPs towards the electrode surface. This is supported by the absence of Warburg impedance in the Randle's equivalent circuit. The EIS results were therefore in agreement with those obtained using chrono-amperometry (CA)

3.3. *Electrochemical properties of modified GCE nano-films*

The CV and DPV voltammograms of drop-coated (DCT) and electro-deposited (EDP) GCE nano-films are as shown in Fig. 5. The voltammograms of the bare GCEs has no peaks indicating their non-electroactivity. However, the CVs of the modified nano-films generally showed typical anodic and cathodic peaks at the indicated potentials. These were in agreement with the corresponding DPV results. The CV of both DCT and EDP GCE/Ag NPs film had characteristic one oxidation and reduction peaks attributable to Ag^0/Ag^+ couples. However, EDP nano-film had broader anodic and cathodic peaks appearing at higher peak potentials compared to DCT. Similar trend was also observed in the DPV results. This suggested that all the electro-deposited Ag NPs on the electrode surface were not stripped off during the anodic scan leading to higher over-potentials. This can also be attributed to diffusion-limited transport of Ag^+ towards the electrode surface due to a thicker film of electro-deposited Ag NPs on the electrode surface. This reduced the rate of reduction of Ag^+ to Ag^0 hence the observed higher peak potentials.

The DCT GCE/Au NPs film had one oxidation and two reduction peaks while EDP GCE/Au NP film had two oxidation and two reduction peaks at slightly lower peak potentials. These were in agreement with the DPV results which also showed two anodic peaks with the DCT peaks being broader than those of EDP nano-films. The appearance of two anodic peaks can be ascribed to surface

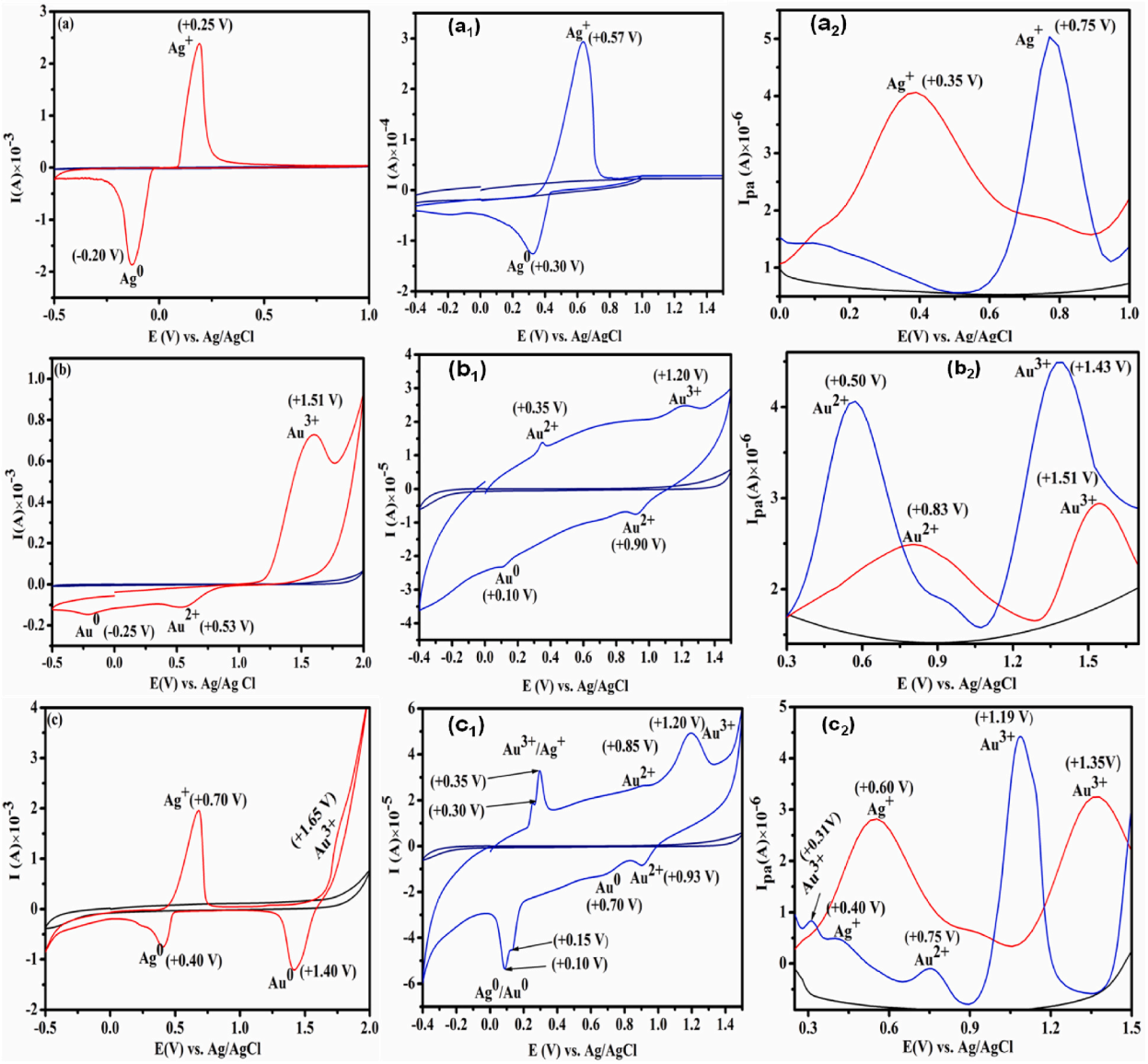

Fig. 5. CVs and DPVs of DCT (**Red**) and corresponding EDP (**Blue**) (a) GCE/Ag NPs, (b) GCE/Au NPs and (c) GCE/Ag-Au (1:2) bimetallic NPs in 0.1 M HCl vs. Ag/AgCl: Scan rate: 30 mVs.

oxidation of Au NPs to form a mixture of Au_2O and Au_2O_3 during the anodic scan. This is in close agreement with reported studies [32]. According to thermodynamics, gold is always oxidized to hydrated gold oxide, Au (OH) $_3$ or Au_2O_3. $3H_2O$ at +1.458 V and to anhydrous gold oxide at + 1.511 V.

with this study. The anodic peak at +1.51 V can be due to the oxidation of Au to Au (OH) $_3$ which was in turn reduced to Au^{2+} at +0.53 V[32]**.** However, these results were not in concordance with studies reported elsewhere [33]. The slight difference can possibly be attributed to the nature of the electrode modification employed in our study which experienced enhanced quantum confinement effects due to the nano-scale size of Au NPs hence the decreased cathodic peak potentials observed. In both GCE/Au NPs films**,** the peak potential separations (ΔE_p) were larger than 0.059 V indicating that the redox reaction of Au NPs was of quasi-reversible type [31].

The CV of DCT GCE/Ag-Au (1:2) NPs had two anodic and two cathodic peaks while those of EDP nano-films had three distinct anodic and cathodic peaks with two similar humps at both anodic and cathodic sides. Both anodic and cathodic peaks of different shapes with significantly low peak current intensities for Au appeared distinctly at different potentials. The Ag peak in the hump was more enhanced in peak current intensity compared to the Au peak. The appearance of the hump indicated the formation of Ag-Au alloy [26].

The DPV of the bimetallic NPs also showed two anodic peaks closely similar to those observed in CVs with the Au^{3+} peak experiencing the highest peak currents. The appearance of the anodic hump observed in the CV was also evident in the DPV at

Table 1
Peak potentials (Epa, Epc), Peak potential separations (ΔEp) and Electrochemical band gaps of drop-coated and electrodeposited Ag NPs, Au NPs and Ag-Au (1:2) NPs.

NPS	Ag		Au		Ag-Au(1:2); Ag(Au)	
modifications	DCT	EDP	DCT	EDP	DCT	EDP
E_{pa} (V)	+0.25	+0.59	+1.51	+1.20	+0.70 (+1.65)	+0.35 (+1.20)
E_{pc} (V)	+0.20	+0.30	+0.53	+0.90	+0.40 (+1.40)	+0.10 (+0.93)
ΔE_p (V)	0.05	0.27	0.98	0.30	0.30 (0.25)	0.25 (0.27)
E^{Θ}	+0.23	+0.44	+1.02	+1.05	+0.55 (+1.53)	+0.23 (+1.07)
E_g^{CV} (eV)	1.34	1.40	1.20	2.05	1.65	2.40

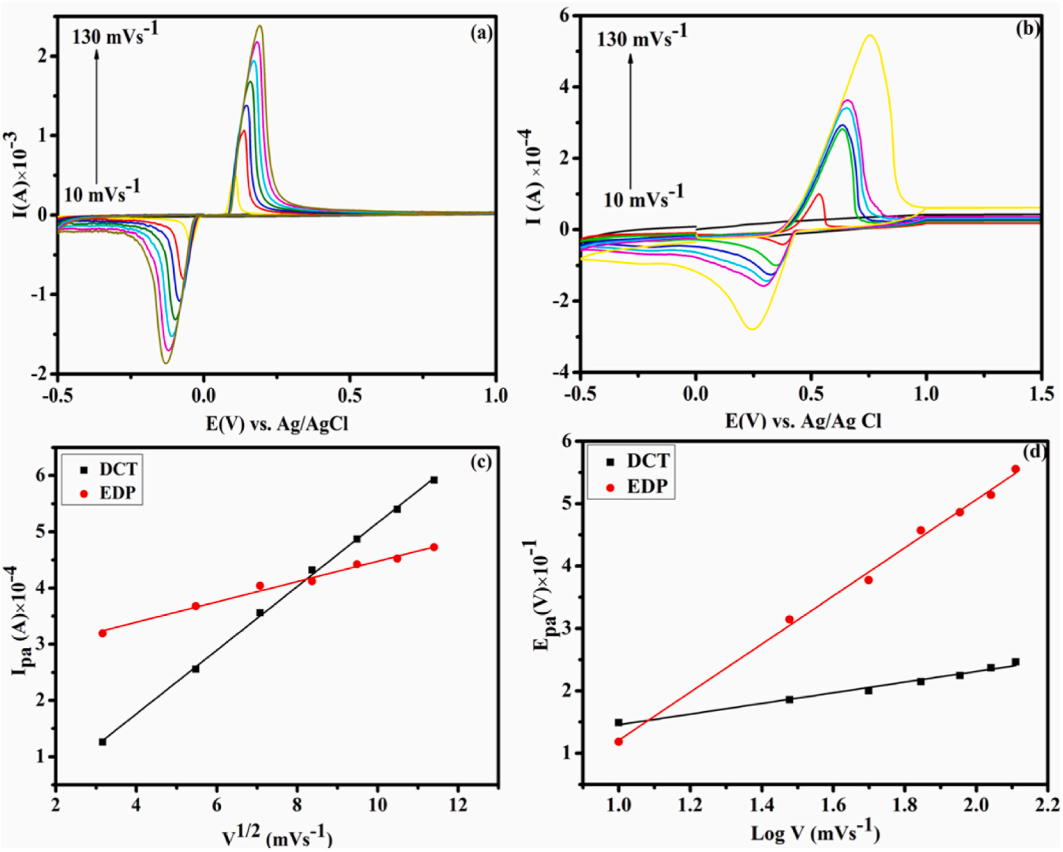

Fig. 6. Scan rate studies of (a) DCT and (b) EDP GCE/Ag NPs, and corresponding (c) *Randle's* and (d) *Laviron's* plots; scan rate: 10-130 mVs^{-1} in 0.1 M HCl vs. Ag/AgCl.

approximately same potentials. This confirmed the sensitivity of DPV technique. The Au^{3+} peak for the DCT nano-film shifted towards more positive potentials. The shapes of the voltammograms in the bimetallic NPs also showed that the redox reaction of Ag NPs was relatively faster than Au NPs with enhanced cathodic and anodic peak currents relative to the EDP nano-film. This is attributed to faster electron transfer rates as depicted by the sharper anodic peaks of DCT GCE/Ag NPs film compared to those of DCT GCE/Au NPs. These electrochemical properties confirmed the major electrical contribution of Ag in the GCE/bimetallic Ag-Au (1:2) NPs film. The electrochemical changes including band gaps for DCT and EDP nano-films as determined using Breda's equation [22] are as shown in Table 1.

The band gap energies (E_g) for DCT and EDP nano-films were in the order: GCE/Au NPs < GCE/Ag NPs < GCE/Ag-Au (1:2) NPs and GCE/Ag NPs < GCE/Au NPs < GCE/Ag-Au (1:2) NPs, respectively. The general trend for EDP E_g was in agreement with the NPs sizes determined using SEM technique described earlier. The increase in E_g can be attributed to the decrease in particle size from Ag NPs to bimetallic Ag-Au (1:2) NPs. The E_g for all DCT nano-films were generally lower than those of corresponding EDP films with the EDP bimetallic nano-film having the largest E_g. This can be ascribed to enhanced quantum confinement effects due to smaller-sized nature of the EDP bimetallic Ag-Au (1:2) NPs [27].

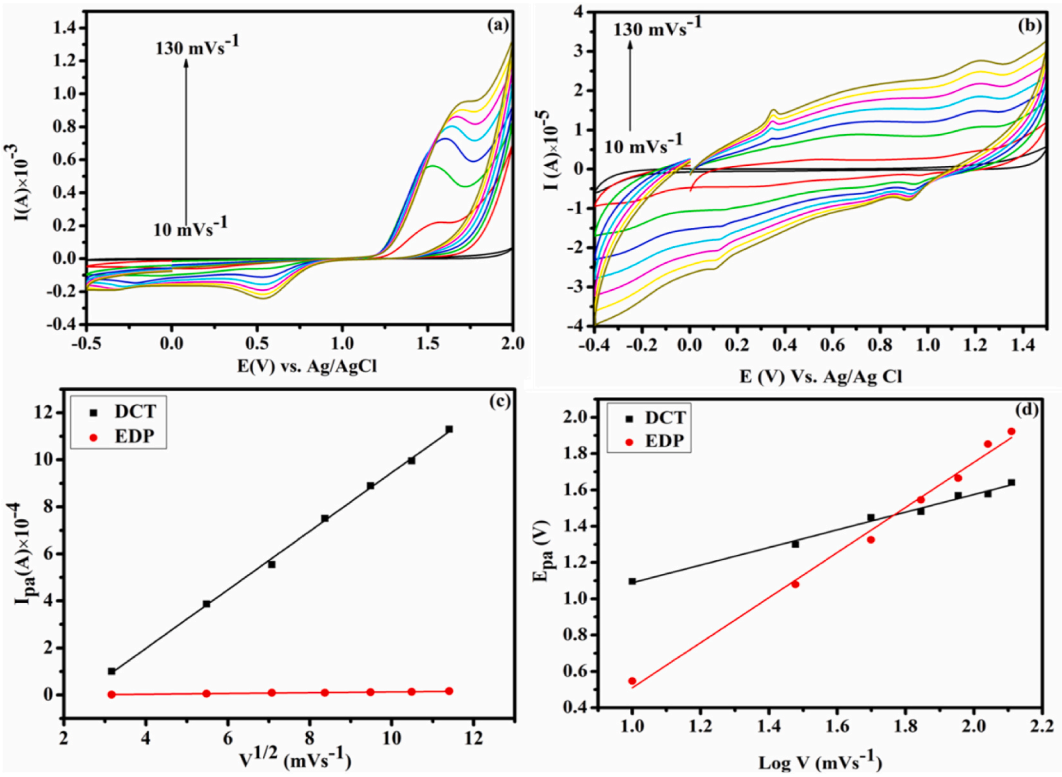

Fig. 7. Scan rate studies of (a) DCT and (b) EDP GCE/Au NPs, and corresponding (c) *Randle's* and (d) *Laviron's* plots; scan rate: 10-130 mVs^{-1} in 0.1 M HCl vs. Ag/AgCl.

3.4. Determination of kinetic parameters for modified GCE nano-films

The CVs for each of the DCT and EDP GCE nano-films showed both anodic and cathodic peaks at different scan rates (Figs. 6–8). The different scan rates were studied using *Randle's* and *Laviron's* plots. This was done so as to determine the electron transfer kinetic parameters including standard heterogenous rate constant (k_s), electron transfer coefficient (α), diffusion coefficient (D), NPs charge contribution and electrode surface coverage (Γ) for each of the modified nano-films using *Laviron's* and *Randle's* equations[37]. The values obtained were tabulated as shown in Table 2.

The I_{pa} for both DCT and EDP GCE/Au NPs films increased linearly with $V^{1/2}$ and significantly higher R^2 values were obtained. However, the R^2 value for the DCT nano-film was greater than EDP. This suggested that the rate of diffusion of Au^{3+} was faster in DCT film relative to the EDP. The E_{pa} for the DCT nano-film also shifted significantly to higher positive values with increasing scan rate compared to EDP. This indicated that the oxidation of Au^0 to Au^{3+} involved more than one step. The Au^0 was first oxidized to Au^{2+} which was finally oxidized to Au^{3+}. This electrochemical behavior of Au is supported by its existence in various oxidation states of +1, +2 and + 3 as similarly described elsewhere [28]. The formation of mixtures of Au oxides during its oxidation to Au^{3+} could have led to slow electron transfer kinetics, uncompensated solution resistance and non-linear diffusion of Au^{3+} towards electrode surface hence the observed shift in potentials to more positive values [29].

The calculated values of α, k_s, Q, Γ and D for both DCT and EDP nano-films varied with EDP film having higher values of k_s and Q while DCT had higher values of α and Γ. Both films had same value for D. However, the values of Q were found to be higher than -2.0×10^{-3} C reported in the literature for colloidal Au NPs [30]. The lower and higher values of k_s and α, respectively for DCT suggested enhanced electron transfer rates as supported by higher Γ. The low value of Γ in EDP film might be attributed to agglomeration of Au NPs on the electrode surface due to its incomplete stripping during the voltametric scans as similarly described elsewhere [34]. The determined value of D for both films can be attributed to their almost equal charge contributions.

The I_{pa} for both DCT and EDP GCE/Ag-Au (1:2) films increased exponentially with $V^{1/2}$ and significantly higher values of R^2 were obtained. The R^2 value due to the effects of Au in EDP nano-film was the greatest compared to Ag in both nano-films. This suggested that higher content of Au in the EDP film enhanced faster rates of diffusion of Au^{3+} relative to its effects in the DCT nano-films. The E_{pa} of both nano-films increased with scan rates. However, the increase was much more distinct and significant in the EDP nano-film with slight positive shift in peak potentials due to the oxidation of Au^{2+} to Au^{3+} compared to DCT film. This is supported by the higher value of R^2 obtained due to the influence of Au in the bimetallic EDP nano-film.

The calculated values of α, k_s, Q, Γ and D for both bimetallic nano-films varied significantly with EDP nano-film due to Au content having the highest values of α and Q. The DCT film due to Au content had higher values of Γ and D. The values of k_s determined were

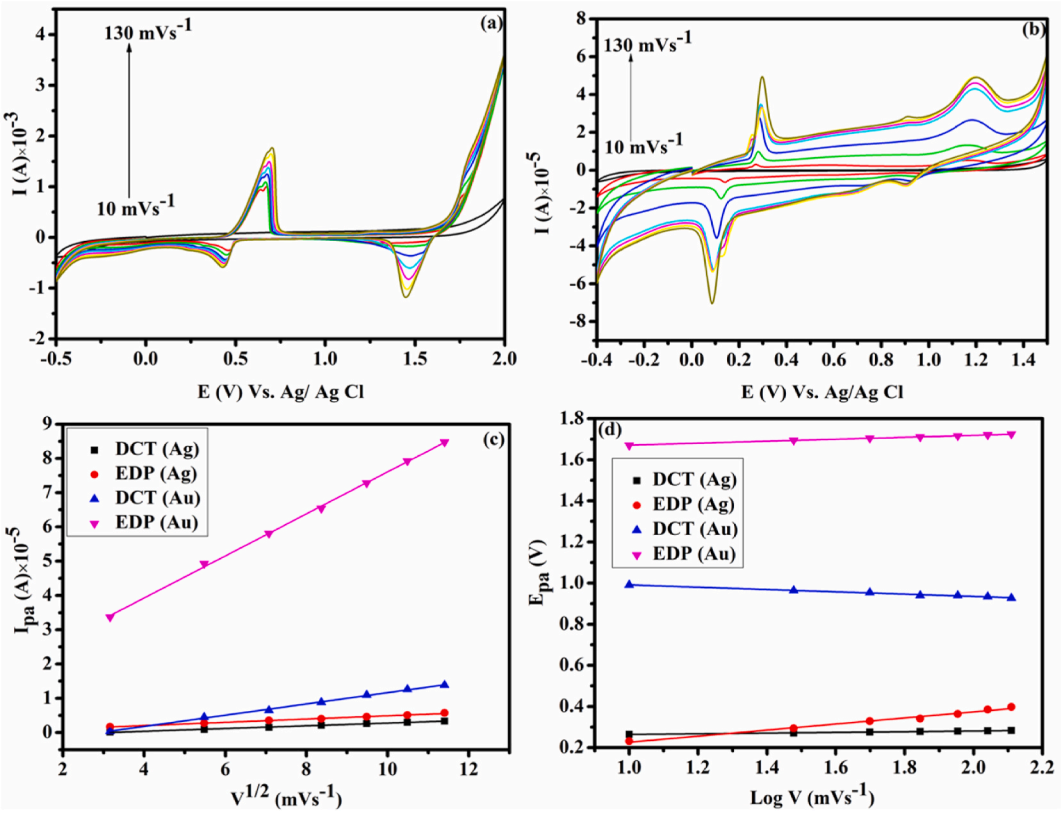

Fig. 8. Scan rate studies of (a) DCT and (b) EDP GCE/Ag-Au (1:2) NPs, and corresponding (c)*Randle's* and (d) *Laviron's* plots; scan rate: 10-130 mVs^{-1} in 0.1 M HCl vs.
Ag/AgCl.

Table 2
Electrochemical kinetic parameters of drop-coated (DCT) and electro-deposited (EDP) nano-films determined from *Randle's* and *Laviron's* equations.

GCE nano-films	Ag		Au		Ag-Au (1:2)	
GCE modifications	DCT	EDP	DCT	EDP	DCT Ag (Au)	EDP Ag (Au)
α	1.16	1.38	0.88	0.82	0.02 (1.64)	0.84 (2.29)
αn	0.12	0.07	0.22	0.47	1.04 (0.39)	0.19 (0.50)
k_s (s^{-1})	0.43	0.26	0.12	0.41	0.01 (0.60)	0.82 (0.59)
Q (C) × (10^{-7})	3.37	2.13	1.90	2.00	4.00 (0.13)	1.00 (9.80)
Γ(molescm^{-2}) × (10^{-11})	4.92	3.11	1.40	1.00	5.00 (7.00)	1.00 (6.55)
D (cm^2s^{-1}) × (10^{-7})	2.10	2.70	7.00	7.00	1.31 (7.34)	0.50 (4.87)
Randle's Plot (R^2)	0.999	0.987	0.998	0.976	0.995 (0.998)	0.996 (0.999)
Laviron's Plot (R^2)	0.983	0.996	0.989	0.992	0.989 0.986)	0.985 (0.998)

found to be within the expected range for normal electrode kinetic processes [32]. The smallest value of k_s due to Ag in the DCT nano-film suggested the availability of electro-active species largely dissolved in the bulk electrolyte [33]. The values obtained for k_s and Q due to Ag and Au contents, respectively in the EDP nano-film indicated faster electron transfer rates relative to the DCT nano-film. This suggested that the electronic structure and surface physiochemistry of the EDP bimetallic nano-film experienced enhanced electron transfer rates [32].

However, its Γ and D values were lower than those of DCT nano-film due to Au content hence significantly experienced slow rates of diffusion of electro-active species towards the electrode surface. The DCT nano-film due to Au content also had higher value of k_s compared to EDP nano-film. The D value of the DCT nano-film was also found to be higher than those reported in the literature [33].

4. Conclusion

The nano films were successful made using chemical and electrochemical modifications of GCE with Ag NPs, Au NPs and bimetallic Ag-Au (1:2) NPs. The chemically modified GCE/Ag-Au (1:2) NPs film had more electrochemical attributes as determined by its CV

analyses compared to electrochemically modified nano-film. The chemically modified GCE nano-films generally showed enhanced values of k_s, Γ and D determined from the experimental data compared to those of electrochemically modified GCE films. There was also an observed increase in intensity for the DCT. Thus suggesting their suitability for applications in various electro-analysis studies. However, the NPS of Au and bimetallic show an increase in peak numbers as well as well resolved peaks in EDP indicative of possible oxidation during electropolymerizing. Hence, from the results it can be concluded that different chemical composition of the metal NPs is formed in the film. There is also a possibility that the EDP mode results in NPs dimensions and morphological changes. Thus, an accurate and thorough optimization of NPs synthesis steps and conditions are necessary to ascertain that the same composition is attained.

CRediT authorship contribution statement

C.O. Duya: Investigation, Formal analysis. **F.O. Okumu:** Supervision, Project administration. **M.C. Matoetoe:** Writing – review & editing, Supervision, Funding acquisition, Conceptualization.

Declaration of competing interest

The authors declare the following financial interests/personal relationships which may be considered as potential competing interests:

Mangaka Matoetoe reports financial support was provided by Water Research Commission.

Acknowledgements

The authors would like to acknowledge Cape peninsula university of Technology (CPUT) and Water Research commission (WRC), South Africa project number K5/2889 for Funding assistance. There is no competing interests on the work and article.

References

[1] C. Gao, Y. Hu, M. Wang, M. Chi, Y. Yin, Fully alloyed Ag/Au nanospheres: combining the plasmonic property of Ag with the stability of Au, J. Am. Chem. Soc. 136 (20) (2014) 7474–7479, https://doi.org/10.1021/ja502890c.
[2] A. Pandikumar, K.S. Devi, Disposable electrochemical sensors for healthcare monitoring, Royal Society of Chemistry 2 (2021). http://ebook.rsc.org/?DOI=10.1039/9781839163364.
[3] J. Sun, L. Liu, F. Yang, A WO3/PPy/ACF modified electrode in electrochemical system for simultaneous removal of heavy metal ion Cu2+ and organic acid, J. Hazard Mater. 394 (12253) (2020) 4, https://doi.org/10.1016/j.jhazmat.2020.122534.
[4] P.S. Adarakatti, S.K. Kempahanumakkagari, Modified electrodes for sensing, Electrochemistry 15 (2019), https://doi.org/10.1039/9781788013895-00058.
[5] Z. Chu, J. Peng, W. Jin, Advanced nanomaterial inks for screen-printed chemical sensors, Sensor. Actuator. B Chem. 243 (2017) 919–926, https://doi.org/10.1016/j.snb.2016.12.022.
[6] L.A. Mercante, M.H.M. Facure, R.C. Sanfelice, F.L. Migliorini, L.H.C. Mattoso, D.S. Correa, One-pot preparation of PEDOT:PSS-reduced graphene decorated with Au nanoparticles for enzymatic electrochemical sensing of H 2 O 2, Appl. Surf. Sci. 407 (2017) 162–170, https://doi.org/10.1016/j.apsusc.2017.02.156.
[7] A.V. Shabalina, V.A. Svetlichnyi, K.A. Ryzhinskaya, I.N. Lapin, Copper nanoparticles for ascorbic acid sensing in water on carbon screen-printed electrodes, Anal. Sci. 33 (12) (2017) 1415–1419, https://doi.org/10.2116/analsci.33.1415.
[8] R.R. Suresh, M. Lakshmanakumar, J.B.B. Arockia Jayalatha, et al., Fabrication of screen-printed electrodes: opportunities and challenges, J. Mater. Sci. 56 (15) (2021) 8951–9006, https://doi.org/10.1007/s10853-020-05499-1.
[9] S. Sadeghi, M. Hemmati, A. Garmroodi, Preparation of Ag-Nanoparticles/Ionic-Liquid modified screen-printed electrode and its application in the determination of metronidazole, Electroanalysis 25 (1) (2013) 316–322, https://doi.org/10.1002/elan.201200412.
[10] L. Jiao, W. Xu, Y. Wu, et al., Single-atom catalysts boost signal amplification for biosensing, Chem. Soc. Rev. 50 (2021), https://doi.org/10.1039/d0cs00367k.
[11] D. Tonelli, E. Scavetta, I. Gualandi, Electrochemical deposition of nanomaterials for electrochemical sensing, Sensors 19 (5) (2019), https://doi.org/10.3390/s19051186.
[12] H.K.S. Yadav, S. Usman, K.A.F. Ghanem, R. Beevi, Synthesis of nanomaterials for drug delivery, Funct Nanomater II 23 (2021) 23–44, https://doi.org/10.1201/9781351021388-2.
[13] Y.H. Chen, R. Kirankumar, C.L. Kao, P.Y. Chen, Electrodeposited Ag, Au, and AuAg nanoparticles on graphene oxide-modified screen-printed carbon electrodes for the voltammetric determination of free sulfide in alkaline solutions, Electrochim. Acta 205 (04.111) (2016) 124–131, https://doi.org/10.1016/j.electacta.2016.
[14] B.D. Anderson, J.B. Tracy, Nanoparticle conversion chemistry: kirkendall effect, galvanic exchange, and anion exchange, Nanoscale 6 (21) (2014) 12195–12216, https://doi.org/10.1039/c4nr02025a.
[15] M.S. Alam, M.F. Shabik, M.M. Rahman, D.M. Valle, M. Hasnat, A Enhanc Electrocatal Eff Pd Part Immobil GC Surf Nitrite Oxid React, vol. 839, 2019, pp. 1–8.
[16] C. Li, Y. Jin, Shell-isolated plasmonic nanostructures for biosensing, catalysis, and advanced nanoelectronics, Adv. Funct. Mater. 31 (7) (2021) 31, https://doi.org/10.1002/adfm.202008031.
[17] G.M. Das, R.V. William, V.R. Dantham, R. Laha, Study on SERS activity of Au-Ag bimetallic nanostructures synthesized using different reducing agents, Phys E Low-Dimensional Syst Nanostructures. 129 (11465) (2021) 6, https://doi.org/10.1016/j.physe.2021.114656.
[18] G. Darabdhara, M.R. Das, S.P. Singh, A.K. Rengan, S. Szunerits, R. Boukherroub, Ag and Au nanoparticles/reduced graphene oxide composite materials: synthesis and application in diagnostics and therapeutics, Adv. Colloid Interface Sci. 271 (10199) (2019) 1, https://doi.org/10.1016/j.cis.2019.101991.
[19] M.S. Holden, K.E. Nick, M. Hall, J.R. Milligan, Q. Chen, C.C. Perry, Synthesis and catalytic activity of pluronic stabilized silver-gold bimetallic nanoparticles, RSC Adv. 4 (94) (2014) 52279–52288, https://doi.org/10.1039/c4ra07581a.
[20] S. Haq, P. Ahmad, M.U. Khandaker, et al., Antibacterial, antioxidant and physicochemical investigations of tin dioxide nanoparticles synthesized via microemulsion method, Mater. Res. Express 8 (3) (2021) 35013, https://doi.org/10.1088/2053-1591/abed8a.
[21] Carry M. William, Rathan S. Vinoth, A. Raja, M. Senthil Pandian, P. Ramasamy, Non-Debye relaxation of AgBiSe2 single crystal featuring flip-flop jumps in Bi valence state, Mater. Lett. 300 (2021) 130179, https://doi.org/10.1016/j.matlet.2021.130179.
[22] J.L. Brédas, R. Silbey, D.S. Boudreaux, R.R. Chance, Chain-length dependence of electronic and electrochemical properties of conjugated systems: polyacetylene, polyphenylene, polythiophene, and polypyrrole, J. Am. Chem. Soc. 105 (22) (1983) 6555–6559, https://doi.org/10.1021/ja00360a004.
[23] M. Verma, M.B. Newmai, P. Senthil Kumar, Synergistic effect of Au-Ag nano-alloying: intense SEIRA and enhanced catalysis, Dalton Trans. 46 (29) (2017) 9664–9677, https://doi.org/10.1039/c7dt02130e.

[24] B. Bonigala, B. Kasukurthi, V.V. Konduri, U.K. Mangamuri, R. Gorrepati, S. Poda, Green synthesis of silver and gold nanoparticles using Stemona tuberosa Lour and screening for their catalytic activity in the degradation of toxic chemicals, Environ. Sci. Pollut. Res. 25 (32) (2018) 32540–32548, https://doi.org/10.1007/s11356-018-3105-9.
[25] J. Liu, Z. Wu, Q. He, Q. Tian, W. Wu, X. Xiao, C. Jiang, Catalytic application and mechanism studies of argentic chloride coupled Ag/Au hollow heterostructures: considering the interface between Ag/Au bimetals, Nanoscale Res. Lett. 14 (2019) 35, https://doi.org/10.1186/s11671-019-2862-9.
[26] S. Akram, J. Castellon, S. Agnel, K. Zhou, J.P. Habas, M.T. Nazir, Multilayer polyimide nanocomposite films synthesis process optimization impact on nanoparticles dispersion and their dielectric performance, J. Appl. Polym. Sci. 138 (4) (2021) 49715, https://doi.org/10.1002/app.49715.
[27] P.N.H. Diem, T.N.M. Phuong, N.Q. Hien, D.T. Quang, T.T. Hoa, N.D. Cuong, Silver, gold, and silver-gold bimetallic nanoparticle-decorated dextran: facile synthesis and versatile tunability on the antimicrobial activity, J. Nanomater. 2020 (2020) 1–11, https://doi.org/10.1155/2020/7195048.
[28] G. Staikov, Nanoscale electrodeposition of low-dimensional metal phases and clusters, Nanoscale 8 (29) (2016) 13880–13892, https://doi.org/10.1039/c6nr01547f.
[29] D. Sharma, J. Lee, J. Seo, H. Shin, Development of a sensitive electrochemical enzymatic reaction-based cholesterol biosensor using Nano-sized carbon interdigitated electrodes decorated with gold nanoparticles, Sensors 17 (9) (2017) 2128, https://doi.org/10.3390/s17092128.
[30] V.A. Isaev, O.V. Grishenkova, Galvanostatic nucleation and growth under diffusion control, J. Solid State Electrochem. 17 (6) (2013) 1505–1508, https://doi.org/10.1007/s10008-013-2119-y.
[31] N.S.K. Gowthaman, B. Sinduja, S.A. John, Tuning the Composition of Gold-Silver Bimetallic Nanoparticles for the Electrochemical Reduction of Hydrogen Peroxide and Nitrobenzene *Electronic Supplementary Material (ESI) for RSC Advances*, This journal is © The Royal Society of Chemistry, 2016.
[32] D.N. Oko, Electrocatalytic Activity of Small Organic Molecules at PtAu Alloy Nanoparticles for Fuel Cells and Electrochemical Biosensing Applications, Université du Québec, 2014. http://espace.inrs.ca/id/eprint/2626.
[33] O. Diaz-morales, F. Calle-vallejo, D.C. Munck, M.T. Koper, Electrochem Water Split by Gold Evid an Oxide Decompos Mech, vol. 4, 2013, pp. 2334–2343.
[34] A. Hassan, S. Ali, M. Muhammad, Cyclic voltammetric study of clarithromycin using gold electrode, Int. Res. J. Pure Appl. Chem. 8 (4) (2015) 221–228, https://doi.org/10.9734/irjpac/2015/18141.